Journal of the Korean Physical Society (2023) 82:522–529
https://doi.org/10.1007/s40042-023-00718-9

Online ISSN 1976-8524
Print ISSN 0374-4884

REVIEW - PARTICLES AND NUCLEI

# Fusion reactions including weakly-bound and halo nuclei around Coulomb barrier

**Kyoungsu Heo**[1] · **Ki-Seok Choi**[2]

Received: 8 September 2022 / Revised: 28 September 2022 / Accepted: 1 October 2022 / Published online: 10 January 2023


**Abstract**
In this study, we investigate fusion cross sections including halo and weakly-bound nuclei around Coulomb barrier. We reviewed our previous results for the total fusion cross sections of the $^{6}$He+ $^{209}$Bi, $^{11}$Li+ $^{208}$Pb and $^{14,15}$C+ $^{232}$Th systems, which involve well-known halo nuclei. Then, to analyze the total fusion reaction of neutron-rich nuclei, $^{9}$Li + $^{70}$Zn system, we introduced the coupled channel method for a two-neutron transfer in the fusion reaction practically. To study the neutron-rich projectile nucleus of this system ($^{9}$Li), we constructed a folding potential with projectile and target densities using charge density distribution. Finally, we analyzed the fusion cross section of the $^{9}$Li + $^{70}$Zn system in one or two channel coupled manners. By adjusting the coupling strength and effective $Q$-value of the coupling form factor, we successfully reproduced the experimental fusion cross-section data for this system. Our results indicate that the two-neutron transfer channel plays a critical role in the fusion reactions of neutron-rich nuclei, such as $^{9}$Li nuclei at energies around the Coulomb barrier.

**Keywords** Coupled-channel method · Total fusion cross section · Light halo nuclei

## 1 Introduction

Over the last two decades, owing to the remarkable advances in radioisotope beam technology, several studies have been performed to measure the total fusion cross sections of systems such as $^{6}$He + $^{209}$Bi [1], $^{6}$Li + $^{209}$Bi [2], $^{11}$Li + $^{208}$Pb [3], $^{9}$Be + $^{208}$Pb [2], and $^{11}$Be + $^{209}$Bi [4] systems. Several theoretical studies on fusion reactions have also been conducted leveraging advances in experimental research, by taking into account typical features of neutron-rich radioisotopes with weak bounds and/or halo structures [2, 5–8]. An efficient theoretical approach to investigate heavy-ion fusion reactions for halo systems is the application of neutron transfer channels to form a coupled channel (CC) [9]. This approach constitutes a practical method to study the effects of weakly bound projectiles comprising a core nucleus and valence neutron(s) in a manner that allows the total fusion cross sections of the halo nucleus on a heavy ion target to be described.

In a previous study [10, 11], we attempted to calculate the fusion cross sections for the $^{11}$Li + $^{208}$Pb, $^{6}$He + $^{208}$Pb, and $^{15}$C + $^{232}$Th systems using the CC method. As a representative halo nucleus, $^{6}$He and $^{11}$Li are weakly bound by two neutrons and the core nucleus, in which $^{11}$Li and $^{6}$He have two-neutron separation energies of $s_{2n} = 0.369$ MeV and 0.975 MeV, respectively [12–14]. Note that the two-neutron separation energy of $^{11}$Li and $^{6}$He is lower than the one-neutron separation energy ($s_n = 0.396$ MeV for $^{11}$Li and $s_n = 1.710$ MeV for $^{6}$He). This implies that if one of the two valence neutrons in these nuclei are removed, the remaining valence neutron should also be immediately separated. It is for this reason that nuclei with structures that have typically been represented by a three-body system, such as $^{11}$Li, have been referred to as "Borromean nuclei" [15–17]. In this paper, we reviewed our previously reported results on the fusion cross sections of the $^{11}$Li + $^{208}$Pb, $^{6}$He + $^{208}$Pb, and $^{15}$C + $^{232}$Th systems in comparison with experimental data.

Additionally, in this work, we investigate the fusion reaction of the $^{9}$Li + $^{70}$Zn systems. The $^{9}$Li nucleus has recently been reported to play an important role in nucleosynthesis. Specifically, the neutron capture reaction, $^{8}$Li(n,$\gamma$)$^{9}$Li, acts as a source for production at mass number A > 8 [18–23]. The

✉ Ki-Seok Choi
kiseokchoi@kau.ac.kr

[1] Department of Physics and Origin of Matter and Evolution of Galaxy (OMEG) Institute, Soongsil University, Seoul 06978, Korea

[2] School of Liberal Arts and Science, Korea Aerospace University, Koyang 10540, Korea

implementation of a CC method in the fusion reaction of the $^{9}$Li + $^{70}$Zn system has already been attempted. The process comprised the application of the two-neutron transfer channel from the $^{11}$Li + $^{68}$Zn system [9, 24]. However, the main goal of this study is to investigate the fusion reaction of the $^{9}$Li + $^{70}$Zn system by simultaneously applying a two-neutron transfer channel CC method to the $^{7}$Li + $^{72}$Zn system in a manner similar to the approach adopted in Ref. [10].

The remainder of this paper is organized as follows. In Sect. 2, we review our previous results for the total fusion cross sections for the $^{6}$He+ $^{209}$Bi, $^{11}$Li+ $^{208}$Pb and $^{15}$C+ $^{232}$Th systems. Then, to analyze the total fusion reaction of the neutron-rich nuclei, $^{9}$Li + $^{70}$Zn system, we introduce the CC method for two-neutron transfer in the fusion reaction described in Sect. 3. Finally, the fusion cross section of $^{9}$Li + $^{70}$Zn system is described and analyzed in Sect. 4. Lastly, we summarize and conclude our discussion in Sect. 5.

## 2 Review of previous results

Firstly, we review systems where the projectile is easily broken by the Borromean structure as $^{6}$He and $^{11}$Li.

To calculate the fusion cross section of the $^{6}$He + $^{209}$Bi system, potential parameters of the Woods–Saxon-type for nuclear attractive potential were applied with global Akyüz-Winther (AW) parameters [25]. In addition, we considered the intrinsic excitation of the projectile and target individually and simultaneously. In the left panel of Fig. 1, the fusion cross section of the $^{6}$He + $^{209}$Bi system is presented. In the figure, the dotted, dot-dashed, long-dashed, and solid lines show the result without any effect, intrinsic excitation of projectile, target, and both nuclei respectively.

Interestingly, the fusion cross section results of the $^{6}$He + $^{209}$Bi system in the left panel in Fig. 1 shows good agreement with the experimental data without any contributions as excitation effects. In general, it is known that global AW parameters provide an accurate description of the total cross section involving stable nuclei for tightly-bound and well-known nuclei. This means that the effect due to the Borromean structure of $^{6}$He did not appear in this experimental data and results. Similar results have been reported previously, where the fusion probability due to the neutron halo of $^{6}$He was not enhanced in the $^{6}$He and $^{238}$U system [26]. More detailed information regarding the calculation of the fusion cross section of the $^{6}$He + $^{209}$Bi system can be found in Ref. [27].

As shown in the right panel of Fig. 1, in contrast to the $^{6}$He + $^{209}$Bi system, the fusion cross section of the $^{11}$Li + $^{209}$Bi system shows large enhancement in fusion probability below the Coulomb barrier, $E_{cm} < 27.3$MeV. In the right panel, the solid line shows the results of the three-channel coupling model with the $^{11}$Li+ $^{208}$Pb, $^{9}$Li+ $^{210}$Pb, and $^{7}$Li+ $^{212}$Pb channels, while the dot-dashed line shows the result obtained by switching off the transfer coupling between $^{9}$Li+ $^{210}$Pb and $^{7}$Li+ $^{212}$Pb. The dotted line shows the results of the single-channel calculation without any coupling effect.

For this theoretical calculation, we constructed the nuclear potential for the $^{11}$Li + $^{208}$Pb system by dividing the core and valance densities for the projectile in folding manner, and calculated the CC equation using the 3-channel approach [10]. In the 3-channel approach, we used the open channel states of $^{9}$Li + $^{210}$Pb system as an intermediate channel for the two-neutron transfer reaction of the $^{11}$Li + $^{208}$Pb system. By applying neutron transfer channels to form a CC, we found that the(multi-) neutron transfer channels play an important role in the fusion reaction of weakly bound nuclei.

Another case of results concerning fusion cross sections including exotic nuclei are fusion cross sections of carbon isotopes and the $^{232}$Th systems [29]. The target of

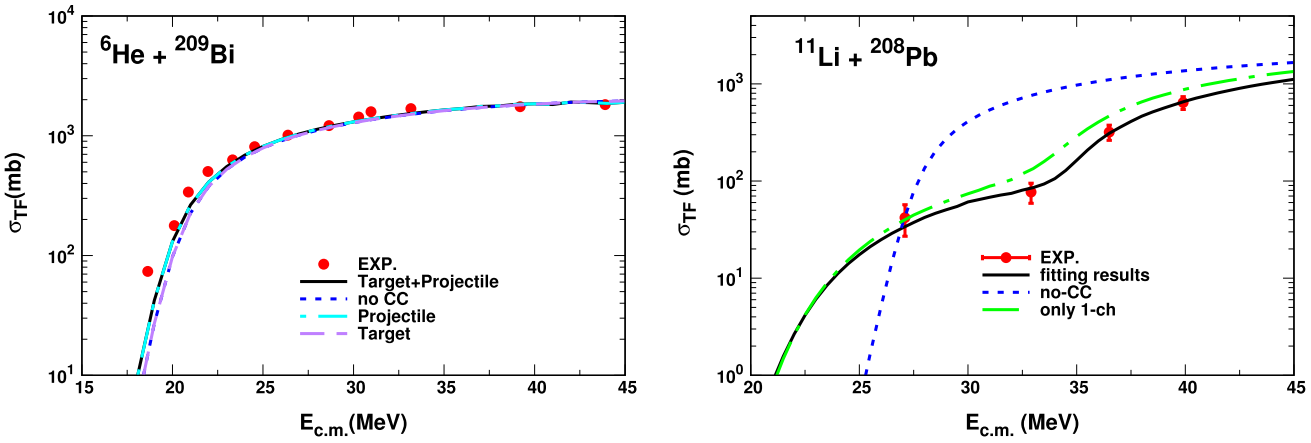


**Fig. 1** Total fusion cross sections of $^{6}$He+ $^{209}$Bi (left panel) and $^{11}$Li+ $^{208}$Pb system(right panel). The experimental data are adopted from Ref. [28] for $^{6}$He+ $^{209}$Bi and Ref. [3] for $^{11}$Li+ $^{208}$Pb system. More details can be found in Refs. [10, 11]

this system, $^{232}$Th, is a well-known deformed nucleus and $^{15}$C in carbon isotopes is known for its one-neutron halo nucleus. For this calculation, we used the deformed Wood-Saxon potential for considering the target deformation, and constructed the folding potential divided by the core part, $^{14}$C and one valance neutron.

The left panel in Fig. 2 shows the fusion cross section of the $^{14}$C + $^{232}$Th system, which leveraged the interaction between the core and target interaction to probe the fusion cross section of the $^{15}$C+$^{232}$Th system. For this calculation, the radius and diffuseness parameters in the Wood-Saxon shape potential were set equivalent to that of the global AW potential. Moreover, the depth of the potential, $V_0$, was adjusted slightly for fitting with the measured fusion cross section.

In the left panel of Fig. 2, the blue dashed line shows the cross section without the deformation effect, and the black solid line shows the cross sections with the deformation effect. Below the Coulomb barrier region,$E_{cm} < 61.48$MeV, we identified the enhancement of the fusion cross sections, taking into account the deformation of $^{232}$Th. The deformation plays an important role in this system.

The right panel of Fig. 2 presents a comparison between the calculated fusion cross sections and experimental data. For the calculation of the total fusion cross-section of the $^{15}$C + $^{232}$Th system, we considered several effects as halo, deformation, and transfer effects simultaneously. The red circles and blue stars show the experimental data for the $^{15}$C + $^{232}$Th and $^{14}$C + $^{232}$Th systems, respectively. The violet dot-dashed curve shows the results for the $^{14}$C + $^{232}$Th system, which is the same as the solid line in left panel of Fig. 2 for comparison. The orange long-dashed curve shows the results for the $^{15}$C + $^{232}$Th system including only the target deformation, in which the result is simply scaled with respect to the radius from that for the $^{14}$C + $^{232}$Th system. The brown dotted line denotes the result obtained by adding the folding potential between one valance neutron and the deformed target, considering the halo effect. As seen in this result, the halo effect admits a large enhancement of fusion cross section below the Coulomb barrier, but shows overestimated results around $E_{cm} \sim 60$ MeV. Finally, the result indicated by the black solid line shows the two-channel CC results considering the one-neutron transfer effect, which shows good agreement with experimental data.

These results highlight that to understand fusion reactions including weakly-bound and halo nuclei, effects such as valance nuclei, transfer, and deformation are crucial.

## 3 Formalism

We adopted a proper CC approach to analyze the experimental fusion data for the $^{9}$Li + $^{70}$Zn system. In general, we have to consider the effects of collective excitations in the colliding nuclei. However, as demonstrated previously [31], the effects of the collective excitations are insignificant in the $^{9}$Li + $^{70}$Zn system. Thus, for simplicity, we have decided to ignore the effects of collective excitations in this system.

We used a CC equation for the two-neutron transfer channels to investigate the effects of such a process [6, 32]. The two-channel coupled equation used in this study is given as

$$\begin{pmatrix} K + V_1 - E & F_{1\to 2}(r) \\ F_{1\to 2}(r) & K + V_2 - (E - Q_{12}) \end{pmatrix} \begin{pmatrix} \psi_1 \\ \psi_2 \end{pmatrix} = 0\,, \qquad (1)$$

where channels 1 and 2, which are denoted by subscripts 1 and 2 respectively in Eq. (1), refer to a ground-state channel of the $^{9}$Li + $^{70}$Zn system and a single effective channel in the $^{7}$Li + $^{72}$Zn system related to the two-neutron transfer. Here, the single effective channel means an arbitrary channel satisfying the effective $Q$-value range for the two-neutron

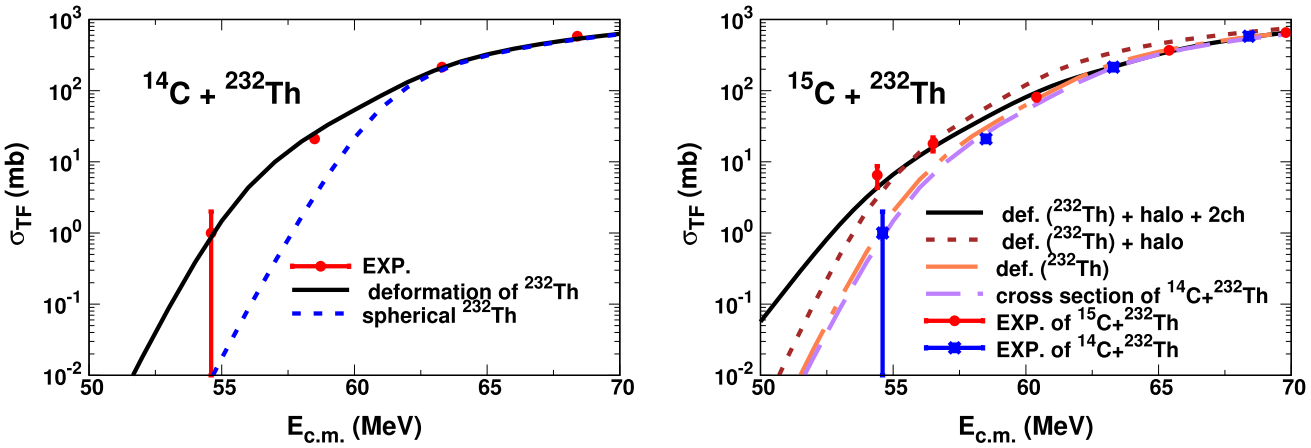


**Fig. 2** The total fusion cross sections of $^{14}$C+ $^{232}$Th (left panel) and $^{15}$C+ $^{232}$Th system(right panel). Both experimental data were adopted from Ref. [30]. More details can be found in Ref. [29]

transfer. In Eq. (1), $K$ is the kinetic energy with a centrifugal potential, $V_i(i = 1, 2)$ is the inter-nuclei potential for each channel, and $Q_{12}$ is the effective $Q$-value for the two-neutron transfer channel, which is determined by fitting to the experimental fusion cross sections. In addition, $F_{1\to2}(r)$ is the coupling form factor which involves the coupling strength and the position with second channel and determined by fitting with experimental data.

To obtain the nuclear potential components of $V_i$(r), we applied two types of potentials for comparison. As in Ref. [10], one is the AW potential [25], determined globally, and the other is the folding potential using the density of the projectile and target as follows

$$V(r) = \int d\mathbf{r}_1 \int d\mathbf{r}_2 \rho_p(r_1)\rho_t(r_2)v_{NN}\left(\left|\mathbf{r} - \mathbf{r}_1 + \mathbf{r}_2\right|\right), \quad (2)$$

where $\rho_p(r_1)$ and $\rho_t(r_2)$ are the density distribution for the projectile and target nuclei, respectively. For the effective nucleon–nucleon interaction, $v_{NN}$, we employ the M3Y interaction [33–35] given by

$$v_{NN}(r) = -2134\,\frac{e^{-2.5r}}{2.5r} + 7999\,\frac{e^{-4r}}{4r} - 275.81\,\delta(\mathbf{r}), \quad (3)$$

in units of MeV.

For the density distribution of the projectile and target nuclei, we employed charge density distribution parameters and density models presented in Ref. [36]. As presented in Ref. [36], we applied the harmonic-oscillator(HO) model for the projectile, $^{7,9}$Li, which has the following form

$$\rho(r) = \rho_0\left(1 + \alpha(r/a)^2\right)\exp(-(r/a)^2), \quad (4)$$

where $a$ and $\alpha$ are parameters in HO model. Moreover, the two parameter Fermi (2pF) model for the target, $^{70,72}$Zn, has the following form

$$\rho_t(r) = \frac{\rho_0}{1 + \exp\left(\frac{r-c}{z}\right)}, \quad (5)$$

where $r$ and $c$ are parameters in 2pF model.

In density distributions of projectile and target, the density parameter, $\rho_0$, is determined by satisfaction of the normalization of the mass distribution as

$$4\pi \int \rho(r)r^2 dr = M, \quad (6)$$

where M is mass of projectile or target nuclei with the uniformed charge distribution assumption.

Then we calculate densities for the projectile and target with the parameters listed in Table 1 taken from Ref. [36], and present the differences in the shapes of each density in Fig. 3.

Using Eq. (2), we can estimate the folding potential of the $^{9}$Li + $^{70}$Zn and $^{7}$Li + $^{72}$Zn systems by the overlap of

**Table 1** Charge density distribution parameters to construct the folding potential in Ref. [36]. In the table, HO and 2pF of the model refer to the harmonic oscillator and two parameter Fermi model, respectively. Moreover, $a$, and $\alpha$ are parameters of HO model for projectile, $^{7,9}$Li in Eq. (4) and $c$, and $z$ are parameters of 2pF model for target, $^{70,72}$Zn in Eq. (5). The numbers in parentheses are error values

| Nucleus | Model | $c$ or $a$ (fm) | $z$ or $\alpha$(fm) |
|---|---|---|---|
| $^{7,9}$Li | HO | 1.77(2) | 0.327 |
| $^{70,72}$Zn | 2pF | 4.426(37) | 0.551(8) |

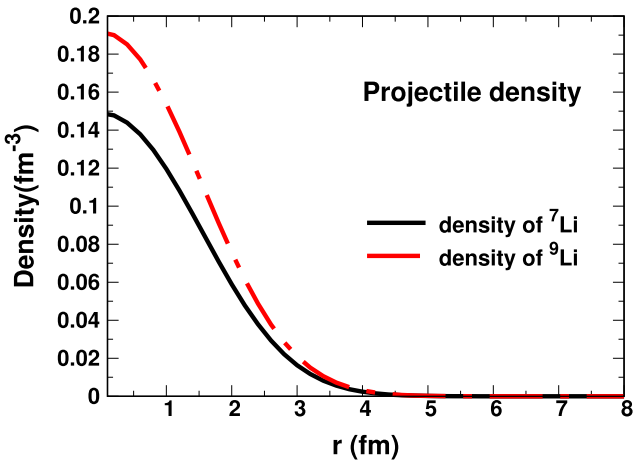


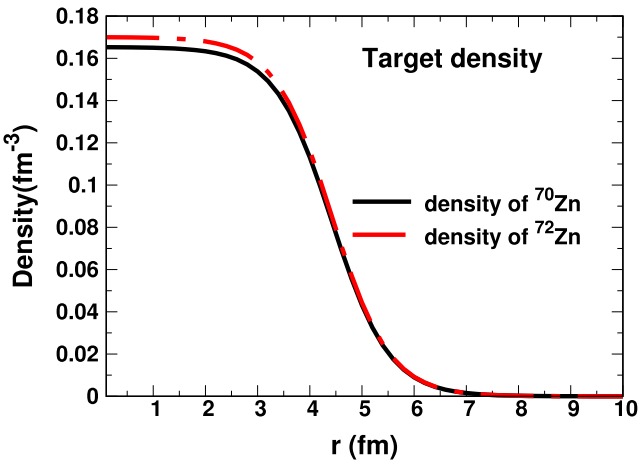


**Fig. 3** Densities of $^{7,9}$Li and $^{70,72}$Zn for construction of folding potentials. In the left panel, the black solid line is the density of $^{7}$Li, and the red dot-dashed line is the density of $^{9}$Li. In the right panel, the black solid line is the density of $^{70}$Zn, and the red dot-dashed line is the density of $^{72}$ Zn. Parameters for these densities are presented in Table 1

densities, and they are indicated by the black solid line in Fig. 4. As presented in Fig. 3, the densities of the projectile, $^{7,9}$Li, show large differences around the surface area, but those of the target, $^{70,72}$Zn, are similar. Therefore, via the contribution of the surface of the projectile density, the depth of the folding potential of the $^{9}$Li + $^{70}$Zn system presents deeper than the case of $^{7}$Li + $^{72}$Zn system.

Using folding potentials of $^{7}$Li+ $^{72}$Zn and $^{9}$Li+ $^{70}$Zn system, we fitted folding potential to Wood-Saxon(WS) form to treat usably, and fitted results are presented red solid lines in Fig 4. The determined parameters by WS fitting process for the potentials of $^{7}$Li+ $^{72}$Zn and $^{9}$Li+ $^{70}$Zn are listed in Table 2, and we treat fitted WS potentials as folding potentials.

For comparison of dependence of potentials, we present that folding potentials and AW potentials for calculation of fusion cross section using 2-channel coupled channel method. In the Table 2, AW refers to the AW potential, which is globally determined by the masses and charges of the considered system. Moreover, folding refers to the fitted folding potential using the WS potential indicated by the red solid line in Fig. 4. Note that the fitted folding potential shows a deeper depth, $V_0$, than that of the AW potential, due to the properties of the original folding potential. Using these parameters, we then calculated the height, position, and curvature of the Coulomb barrier, and the results are presented in table II.

## 4 Results

In Fig. 5, we present the results of total cross sections of the $^{9}$ Li+$^{70}$Zn system obtained by the one and two-channel coupled model with two types of different potentials parameterized in table. II.

First, we compare results for the one-channel calculation for AW parameters (cyan dot-dot-dashed line) and for the fitted folding potential (blue dotted line). Although the predictions of both models have large discrepancies in comparison with experimental data at low energy region, one-channel of folding potential case has better agreement with experimental data in $E_{cm} > 12$MeV region.

In addition, the intrinsic excitation effect is presented using dotted line on the fitted folding potential basis (green

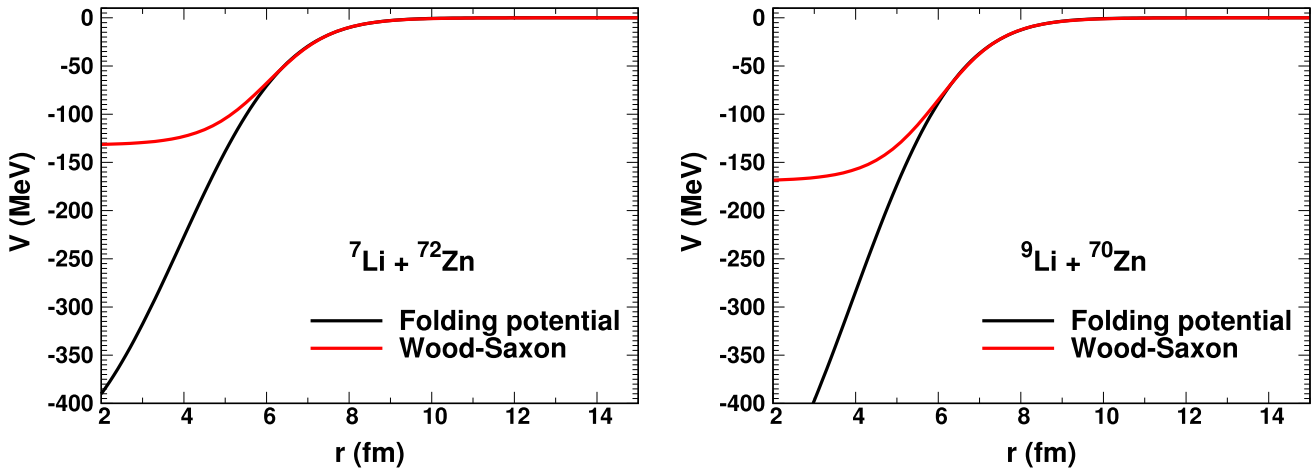


**Fig. 4** Folding potentials of $^{7}$Li+ $^{72}$Zn (left panel) and $^{9}$Li+ $^{70}$Zn system (right panel). Both solid black lines indicate calculations of the folding potential using Eq. (2), and red solid lines are fitted via the Wood-Saxon potential

**Table 2** Depth($V_0$), radius($r_0$), and diffuseness($a_0$) parameters for the nuclear Woods–Saxon shape potential for each channel in the $^{9}$Li + $^{70}$Zn and $^{7}$Li + $^{72}$Zn reaction systems. In the table, AW means that global Akyüz-Winther (AW) parameters and folding means that fitted folding potential using WS potential. The corresponding barrier height, $V_b$, barrier position $R_b$, and barrier curvature $\hbar\Omega$ are also presented for each potential

| Channel | $V_0$ (MeV) | $r_0$ (fm) | $a_0$ (fm) | $V_b$ (MeV) | $R_b$ (fm) | $\hbar\Omega$ (MeV) |
|---|---|---|---|---|---|---|
| $^{9}$Li + $^{70}$Zn (Channel 1 AW) | 43.396 | 1.171 | 0.618 | 12.5 | 9.7 | 3.12 |
| $^{7}$Li + $^{72}$Zn (Channel 2 AW) | 42.310 | 1.170 | 0.608 | 12.82 | 9.4 | 3.59 |
| $^{9}$Li + $^{70}$Zn (Channel 1 folding) | 169.364 | 0.969 | 0.785 | 11.92 | 10.02 | 2.67 |
| $^{7}$Li + $^{72}$Zn (Channel 2 folding) | 132.054 | 0.995 | 0.780 | 12.17 | 9.80 | 3.05 |

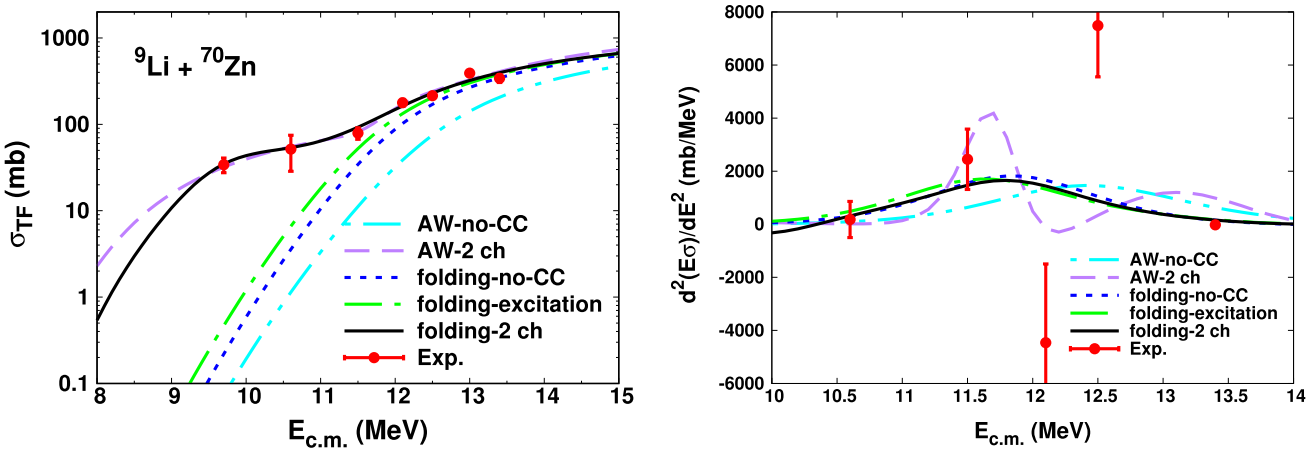


**Fig. 5** Total fusion cross sections (left panel), and fusion barrier distribution, $d^2(E\sigma)/dE^2$ (right panel), for the $^9$Li + $^{70}$Zn system. The black solid and violet long-dashed lines denote the results of the two-channel calculations with folding and AW potentials, respectively. The results of the one-channel calculations are denoted by blue dotted and cyan dot-dot-dashed lines for each potential. The results represented as green dot-dashed lines were obtained by taking into account the collective excitations in the colliding nuclei in the one-channel calculations of the folding potential. The experimental data were adopted from Ref. [31]

dot-dashed line). Regarding the collective excitations, the rotational excitation corresponding to the first excited state of $^9$Li (2.69 MeV) was determined to be associated with a quadrupole deformation parameter value of $\beta_2 = 0.469$. The vibrational coupling to the $2^+$ state in $^{70}$Zn at 0.884 MeV yielded the deformation parameter $\beta_2 = 0.228$ [31]. The effects of the collective excitations can be considered insignificant, because the differences between the results with and without considering the collective excitations were small in the case of the one-channel calculation of the folding potential. These results are similar to those reported in Ref. [37].

For constructing the two-channel coupling effect, we employ a proper form factor for connecting channels as presented $F_{1\to2}(r)$ in Eq. (1). In this work, the coupling form factor $F_{1\to2}(r)$ in Eq. (1) is considered as a derivative form of the Woods–Saxon potential [38], as follows:

$$F_{1\to2}(r) = F_t \frac{d}{dr}\left(\frac{1}{1+\exp((r-R_{\rm coup})/a_{\rm coup})}\right). \quad (7)$$

To optimize the four adjustable parameters ($F_t$, $R_{\rm coup}$, $a_{\rm coup}$, and $Q_{12}$) related to the coupling form factor and $Q$-value, we applied a $\chi$-square fitting process to the experimental fusion cross-section data of $^9$Li + $^{70}$Zn system in Ref. [31]. The fitted values for these parameters are also listed in Table 3. It is worth noting that the $Q$-value for the ground-state-to-ground state transition of $^{70}$Zn($^9$Li,$^7$Li)$^{72}$Zn was $Q_{gg} = +8.6$ MeV. In table III, the coupling strength, $F_t$, of the AW potential is significantly stronger than that of the folding potential, because the AW potential of the one-channel for $^9$Li+$^{70}$Zn system is underestimated.

**Table 3** Effective transfer $Q$-value and parameters for the coupling form factor given by Eq. (2). The values were obtained by fitting the results of the coupled-channel calculations to the experimental data

| reaction | $Q_{12}$ (MeV) | $F_t$ (MeV fm) | $R_{\rm coup}$ (fm) | $a_{\rm coup}$ (fm) |
|---|---|---|---|---|
| $^9$Li + $^{70}$Zn (AW) | 4.471 | 13.353 | 2.304 | 0.940 |
| $^9$Li + $^{70}$Zn (Folding) | 2.74 | 2.49 | 2.573 | 0.693 |

Using the introduced coupling form factor and parameters, we analyzed the fusion cross sections of the $^9$Li+$^{70}$Zn system including the two-channel coupled effect, which is effectively considered two-neutron transfer. The black solid and violet long-dashed lines in Fig. 5 denote the results of the two-channel calculations with folding and AW potentials, respectively. Both lines show good agreement with the experimental data. This means that the contribution of the two-neutron transfer channel is more significant below the Coulomb barrier region, $E_{cm} < 12.5$MeV. The large contribution of coupled channel effect in this calculation means that the consideration of other channels except coupling with excitation state as break up or transfer channels is essential in the $^9$Li+$^{70}$Zn system although we could not distinguish break up and transfer channel in this simple model.

Also, the difference is that the case of folding potential is underestimated than that of AW potential in low energy region, $E_{cm} < 9$MeV. It shows that the determination of potential is crucial in sub-barrier region, $E_{cm} < 9$MeV.

In the view of fusion barrier distribution, it is more distinguishable. The right panel of Fig. 5 shows the fusion barrier distribution defined as $d^2(E\sigma)/dE^2$ [39] with the same

legend. The fusion barrier distribution of the experimental data was obtained from the experimental fusion cross section presented in the left panel of Fig. 5 using a point-difference formula. One can see that the peak energies of the barrier distributions are varied by potential and included effects. The case of the two-channel calculation with AW potential shows large difference with others, because of the strongly coupled effect with the two-neutron transfer channel with the presented parameters in table III. In these results, the transfer effect is important, and folding potential works well. However, estimations under the Coulomb barrier region, $E_{cm} < 12.5$MeV, are uncertain. Thus, to fill this knowledge gap, we need to perform further research using other experimental data.

## 5 Summary and conclusions

We analyze results of fusion reaction including exotic nuclei such as weakly-bound and halo nuclei in the barrier penetration model. First, we reviewed previous fusion reaction results including halo nuclei such as $^{6}$He, $^{11}$Li, and $^{15}$C, which are well-known one- and two-neutron halo nuclei using the CC method.

We conducted a phenomenological study on the fusion cross sections of $^{9}$Li + $^{70}$Zn system practically. An important difference of fusion cross sections between other systems including stable nuclei is the unusual increase in the fusion cross sections at energies below the Coulomb barrier. To better understand the reason why relatively large fusion cross sections exist at energies below the Coulomb barrier of the system, we employed a CC approach comprising a one-channel and a two-neutron transfer channel.

Using the method of global AW parameterization and folding potential description using densities of projectile and target, we determined the potential parameters for two coupled channels. By adjusting the effective two-neutron transfer $Q$-values and the parameters for the coupling form factors, we successfully reproduced the experimental fusion cross sections.

We found that taking into account only one-channel mode, both with or without consideration of the excitation states resulted in underestimation of the experimental data. However, the experimental data were well represented by taking into account two-neutron transfer channel coupling.

More measurements of the fusion cross sections including halo and weakly-bound nuclei at energies below the Coulomb barrier would be needed for understanding fusion mechanisms including halo and weakly-bound nuclei, and we expect that our progress would be helpful to analyze future experimental data.

**Acknowledgements** The authors wish to express their sincere gratitude to Professor K. Hagino for providing valuable comments. This work was supported by the National Research Foundation of Korea (Grant No. NRF-2021R1F1A1051935).

## References

1. A. Hassan, Bull. Rus. Acad. Sci. Phys. **70**, 1558 (2006)
2. M. Dasgupta, P.R.S. Gomes, D.J. Hinde, S.B. Moraes, R.M. Anjos, A.C. Berriman, R.D. Butt, N. Carlin, J. Lubian, C.R. Morton, J.O. Newton, A. Szanto de Toledo, Phys. Rev. C **70**, 024606 (2004)
3. A.M. Vinodkumar, W. Loveland, R. Yanez, M. Leonard, L. Yao, P. Bricault, M. Dombsky, P. Kunz, J. Lassen, A.C. Morton, D. Ottewell, D. Preddy, M. Trinczek, Phys. Rev. C **87**, 044603 (2013)
4. C. Signorini, A. Yoshida, Y. Watanabe, D. Pierroutsakou, L. Stroe, T. Fukuda, M. Mazzocco, N. Fukuda, Y. Mizoi, M. Ishihara, H. Sakurai, A. Diaz-Torres, K. Hagino, Nucl. Phys. A **735**, 329 (2004)
5. K. Hagino, A. Vitturi, C.H. Dasso, S.M. Lenzi, Phys. Rev. C **61**, 037602 (2000)
6. K. Hagino, N. Takigawa, Prog. Theor. Phys. **128**, 1061 (2012)
7. L. Canto, P. Gomes, R. Donangelo, M. Hussein, Phys. Rep. **424**, 1 (2006)
8. L. Canto, P. Gomes, R. Donangelo, J. Lubian, M. Hussein, Phys. Rep. **596**, 1 (2015)
9. V.I. Zagrebaev, V.V. Samarin, W. Greiner, Phys. Rev. C **75**, 035809 (2007)
10. K.-S. Choi, M.-K. Cheoun, W.Y. So, K. Hagino, K.S. Kim, Phys. Lett. B **780**, 455 (2018)
11. K.-S. Choi, M.-K. Cheoun, K.S. Kim, T. Kim, W.Y. So, J. Korean Phys. Soc. **70**, 42 (2017)
12. N. Takigawa, H. Sagawa, Phys. Lett. B **265**, 23 (1991)
13. C. Forssén, V.D. Efros, M.V. Zhukov, Nucl. Phys. A **706**, 48 (2002)
14. F. Barranco, E. Vigezzi, R. Broglia, Phys. Lett. B **319**, 387 (1993)
15. J. Bang, B. Danilin, V. Efros, J. Vaagen, M. Zhukov, I. Thompson, Phys. Rep. **264**, 27 (1996)
16. T. Myo, S. Aoyama, K. Katō, K. Ikeda, Phys. Lett. B **576**, 281 (2003)
17. S. Kumar, V.S. Bhasin, Phys. Rev. C **65**, 034007 (2002)
18. J. Görres, H. Herndl, I.J. Thompson, M. Wiescher, Phys. Rev. C **52**, 2231 (1995)
19. V.D. Efros, W. Balogh, H. Herndl, R. Hofinger, H. Oberhummer, Z. Phys. A **355**, 101 (1996)
20. S.B. Dubovichenko, A.V. Dzhazairov-Kakhramanov, Astrophys. J. **819**, 1 (2016)
21. T. Kajino, G. Mathews, G. Fuller, Astrophys. J. **364**, 7 (1990)
22. R. Malaney, W. Fowler, in *The origin and distribution of the elements*. ed. by G.J. Mathews (World Scientific, Singapore, 1988)
23. P. Banerjee, R. Chatterjee, R. Shyam, Phys. Rev. C **78**, 035804 (2008)
24. A. Balantekin, G. Kocak, AIP Conf. Proc. **1072**, 289 (2008)
25. Ö. Akyüz, A. Winther, Proceedings of the Enrico Fermi School of Physics. 1979, (1981)
26. Riccardo Raabe, J.L. Sida, J.L. Charvet, N. Alamanos, C. Angulo, J.M. Casandjian, S. Courtin, A. Drouart, D.J.C. Durand, P. Figuera et al., Nature **431**, 823 (2004)
27. K.-S. Choi, M.-K. Cheoun, K.S. Kim, T.H. Kim, W.Y. So, J. Korean. Phys. Soc. **70**, 42 (2017)
28. A. A. Hassan, S. Lukyanov, R. Kalpakchieva, Yu. E. Penionzhkevich, R. A. A. stabatyan, J. Vinsour, Z. Dlouhy, A. A. Kulko, J. Mrazek, S. P. Lobastov, E. R. Markaryan, V. A. Maslov, N. K.

Skobelev, Yu. G. Sobolev, Bull. Rus. Acad. Sci. Phys. **70**, 1558 (2006)
29. K.-S. Choi, K.S. Kim, M.-K. Cheoun, W.Y. So, K. Hagino, Phys. Rev. C **103**, 034611 (2021)
30. M. Alcorta, K.E. Rehm, B.B. Back, S. Bedoor, P.F. Bertone, C.M. Deibel, B. DiGiovine, H. Esbensen, J.P. Greene, C.R. Hoffman, C.L. Jiang, J.C. Lighthall, S.T. Marley, R.C. Pardo, M. Paul, A.M. Rogers, C. Ugalde, A.H. Wuosmaa, Phys. Rev. Lett. **106**, 172701 (2011)
31. W. Loveland, A.M. Vinodkumar, R.S. Naik, P.H. Sprunger, B. Matteson, J. Neeway, M. Trinczek, M. Dombsky, P. Machule, D. Ottewell, D. Cross, K. Gagnon, W.J. Mills, Phys. Rev. C **74**, 064609 (2006)
32. K. Hagino, N. Rowley, A. Kruppa, Comput. Phys. Commun. **123**, 143 (1999)
33. G. Bertsch, J. Borysowicz, H. McManus, W. Love, Nucl. Phys. A **284**, 399 (1977)
34. G. Satchler, W. Love, Phys. Rep. **55**, 183 (1979)
35. G. Satchler, Nucl. Phys. A **329**, 233 (1979)
36. H. De Vries, C.W. De Jager, C. De Vries, At. Data Nucl. Data Tables **36**, 495 (1987)
37. A.M. Vinodkumar, W. Loveland, P.H. Sprunger, L. Prisbrey, M. Trinczek, M. Dombsky, P. Machule, J.J. Kolata, A. Roberts, Phys. Rev. C **80**, 054609 (2009)
38. C. Dasso, G. Pollarolo, Phys. Lett. B **155**, 223 (1985)
39. N. Rowley, G. Satchler, P. Stelson, Phys. Lett. B **254**, 25 (1991)